Applied Catalysis B: Environmental 232 (2018) 117–123

Contents lists available at ScienceDirect

Applied Catalysis B: Environmental

journal homepage: www.elsevier.com/locate/apcatb

Molybdenum disulfide quantum dots decorated bismuth sulfide as a superior noble-metal-free photocatalyst for hydrogen evolution through harnessing a broad solar spectrum

W.P. Cathie Lee[a], Xin Ying Kong[a], Lling-Lling Tan[b], Meei Mei Gui[c], S. Sumathi[d], Siang-Piao Chai[a,*]

[a] Multidisciplinary Platform of Advanced Engineering, Chemical Engineering Discipline, School of Engineering, Monash University, Jalan Lagoon Selatan, 47500, Bandar Sunway, Selangor, Malaysia
[b] School of Engineering and Physical Sciences, Heriot-Watt University Malaysia, Jalan Venna P5/2, Precinct 5, 62200, Putrajaya, Malaysia
[c] Nanotechnology and Integrated Bioengineering Centre, University of Ulster, Belfast, BT37 0BQ, Northern Ireland, United Kingdom
[d] Faculty of Engineering and Green Technology, Universiti Tunku Abdul Rahman, Kampar Campus, Jalan Universiti, Bandar Barat, 31900, Kampar, Perak, Malaysia

ARTICLE INFO

Keywords:
Hydrogen
Broad solar spectrum
Quantum dots
Photocatalyst
Molybdenum disulfide

ABSTRACT

Molybdenum disulfide quantum dots (MoS_2QDs) decorated bismuth sulfide (Bi_2S_3) photocatalyst was synthesized. Photoluminescence characterization showed that the as-developed MoS_2QDs possessed intriguing up-conversion and down-conversion properties, indicating their capability to harness energy from the light spectrum ranging from ultraviolet (UV) to near-infrared (NIR). In this study, the highest hydrogen yield of 17.7 mmol/g.h was achieved by 0.14MoS_2QD/Bi_2S_3, which was almost 4.5 folds higher than that of undoped Bi_2S_3 under stimulated solar light irradiation. Furthermore, examination of the 0.14MoS_2QD/Bi_2S_3 photocatalysts under NIR irradiation showed a significant photocurrent response and an accumulative H_2 yield of 53.6 μmol/g after 6 h reaction. This is a major breakthrough as most photocatalysts can only be activated under UV and/or visible light irradiation. This work provides new insights into the design of MoS_2QD/Bi_2S_3 for harnessing energy from a broad solar spectrum to photocatalytically split water to produce hydrogen.

1. Introduction

Energy generation by fossil fuel combustion dominates the emission of carbon dioxide (CO_2), the major contributor to climate change and global warming. The rapid industrialization and technological progress that permeates every facet of life have further escalated the rate of fossil fuel depletion and CO_2 emission. Therefore, an alternative fuel source that is both clean and renewable is of paramount importance. Hydrogen (H_2), in particular is a promising candidate to replace fossil fuels owing to its high fuel value of ~143 kJ/g. Furthermore, the combustion of H_2 produces only water as by-product, rendering the process environmentally benign [1].

There are a variety of methods to produce H_2, such as solar energy pyrogenic decomposition, photo-electrochemistry method, photocatalysis and solar energy combined with electrolytic process. Among these routes, the photocatalytic splitting of water to generate H_2 has been widely regarded as one of the most sustainable approaches as the process can be carried out under room temperature and atmospheric pressure, in the presence of light irradiation [2–6]. The redox reaction is initiated by photoexcitation when the energy of photons from the light source is equal to or greater than the band gap of a semiconductor photocatalyst. The electrons are then excited from the valence band (VB) to the conduction band (CB), where these electrons are subsequently consumed to produce H_2. It is therefore crucial to develop an efficient photocatalyst which exhibits suitable redox potentials, broad light absorption, and high photostability throughout the reaction. Noble metals, such as Pt, Pd, Au and Ag, have been studied extensively to achieve high photocatalytic activity for H_2 production [7–11]. However, the scarcity of these precious metals and high production costs limit the practicality of using noble metals for photocatalytic H_2 production. Under such circumstances, it is essential to design and develop an efficient and noble-metal-free photocatalytic system.

In view of solar energy utilization, the search for semiconductor photocatalysts that can harvest the wide spectrum of solar light, from ultraviolet (UV) to near-infrared (NIR) wavelength, and simultaneously achieve efficient solar energy conversion remains as one of the most challenging missions. At present, most photocatalysts developed in literature are active in the UV and/or visible light region, while activity

* Corresponding author.
E-mail address: chai.siang.piao@monash.edu (S.-P. Chai).

https://doi.org/10.1016/j.apcatb.2018.03.019
Received 27 December 2017; Received in revised form 15 February 2018; Accepted 5 March 2018
Available online 07 March 2018
0926-3373/

under NIR light still remains rare. Utilization of light from NIR region can be achieved by converting longer wavelength NIR light to shorter wavelength visible light by means of doping with rare earth materials [12,13]. In addition, surface plasmonic effect possessed by noble metals has also been reported as an NIR harvester for photocatalysis [14,15].

Owing to its unique properties and versatility for numerous applications, molybdenum disulfide (MoS_2), has been gaining tremendous attention from researchers worldwide [16–18]. The crystal structure of MoS_2 consists of sandwiched layers S-Mo-S bonded through covalent bonds and each layer is held together by relatively weak van der Waals forces. MoS_2 with bulk structure has an indirect band gap of *ca.* 1.0 eV, while its direct band gap energy is approximately 1.8–2.0 eV. With this sandwiched structure, MoS_2 comprises of unsaturated Mo and S edges that serve as active sites where they can bond with reactant molecules to initiate surface reactions. However, the limited active sites on the basal plane of MoS_2 have hindered the catalytic efficiency of MoS_2 [19]. Therefore, morphology engineering of MoS_2, such as reducing the number of layers and sizes, has been widely studied in an effort to increase its catalytic activity through edge exposing [19]. By decreasing the layers of MoS_2, the band gap of MoS_2 could be transformed from indirect band gap (~1.0 eV) to direct band gap (1.8–2 0eV) [20,21].

Among the different shapes and sizes of MoS_2, zero-dimensional (0D) MoS_2 quantum dots (MoS_2QDs) possess unique optical and electronic properties, which are vital in many applications, particularly photocatalysis [1,22–25]. The quantum size of MoS_2QDs not only results in an increase in unsaturated bonds, but higher exposed edges per surface area as well. The latter will in turn enable more hydrogen atoms to be bonded to the photocatalyst, thereby increasing the photocatalytic activity for H_2 generation. Furthermore, MoS_2QDs have been reported to exhibit up-conversion properties [26,27].

In our previous study, MoS_2 sheets were grown onto Bi_2S_3 giving a core-shell like structure that was shown to be an efficient photocatalyst for H_2 production [28]. In this study, we further enhanced the performance of Bi_2S_3-based photocatalyst in water splitting with MoS_2QDs under broad solar spectrum. To the best of our knowledge, this is the first time MoS_2QDs has been reported to exhibit photoactivity under NIR light irradiation. The synthesis of MoS_2QDs was carried out *via* a top-down approach with the aid of sonication. The unique and fascinating excitation-dependent photoluminescence emission of MoS_2QDs was also thoroughly examined in this work. The photocatalytic enhancement of MoS_2QD/Bi_2S_3 catalyst revealed the significance of MoS_2 structure in achieving a higher efficiency for H_2 production.

2. Materials and methods

2.1. Materials

Bismuth (III) nitrate pentahydrate ($Bi(NO_3)_3{\cdot}5H_2O$), thioacetamide (C_2H_5NS), N,N-dimethylformamide (DMF), sodium sulfide (Na_2S) and sodium sulfite (Na_2SO_3) were supplied by Sigma Aldrich. Sodium tungstate dihydrate ($Na_2WO_4{\cdot}2H_2O$) and ethanol were supplied from Merck and Friendemann Schmidt Chemical, respectively. All the chemicals were of analytical reagent grade and were used as received without further purification. Deionized (DI) water with conductivity of 18.2 MΩ cm was used in all experiments.

2.2. MoS_2 Quantum dots synthesis

MoS_2 quantum dots (MoS_2QDs) were prepared through a sonochemical method following the procedure reported elsewhere [16] with modifications. In brief, bulk MoS_2 was first dispersed in 100 mL of DMF solution. Next, the MoS_2 suspended solution was placed in an ice-bath and underwent sonication at 300 W for 3 h. The sonicated solution was then left undisturbed overnight to allow the bulk MoS_2 to settle. The top 2/3 of the suspended solution was then extracted to a round bottom flask and heated under reflux to 140 °C for 6 h under constant stirring. The cooled suspension was then centrifuged for 10 min at 5000 rpm to allow the sediment and supernatant to separate. The supernatant was then centrifuged again at 14,000 rpm for 15 min to obtain MoS_2 suspension. The supernatant was collected and dried in a vacuum oven and re-dispersed in DMF to obtain MoS_2QDs suspension with concentration of 8 mg/mL.

2.3. Synthesis of MoS_2QD/Bi_2S_3 photocatalyst

Prior to obtaining MoS_2QD/Bi_2S_3, Bi_2WO_6 was first synthesized by dissolving 0.4 mmol of $Na_2WO_4{\cdot}2H_2O$ and 0.8 mmol of $Bi(NO_3)_3{\cdot}5H_2O$ in 100 mL of DI water under constant stirring for 1 h. The solution was subsequently heated in a Teflon-lined autoclave for 15 h at 160 °C. The precipitate was washed with DI water and ethanol before drying in an oven. The as-synthesized Bi_2WO_6 was then suspended in DI water through sonication for 1 h. Thioacetamide was subsequently added to the suspended solution under constant mixing before adding a pre-calculated amount of MoS_2QDs suspension. The solution was then heated to 200 °C for 24 h in a Teflon-lined autoclave. After allowing the autoclave to cool down naturally, the precipitate was then washed with DI water and ethanol before drying in an oven. The as-prepared samples were denoted as xMoS_2QD/Bi_2S_3, where x = 0.07, 0.14, 0.17, 0.21 and 0.36 wt% of MoS_2QDs content.

2.4. Material characterization

The structural properties of the samples were analyzed by powder X-ray diffraction (XRD) with Bruker D8 Discover X-ray diffractometer with CuKα radiation (λ = 0.15406 nm) at a scan rate of $0.02^{\circ}\,s^{-1}$. Field-emission scanning electron microscope (FE-SEM, Hitachi SU8010) was used to study the surface morphology of the as-prepared samples. Transmission electron microscopy (TEM) and high resolution TEM (HR-TEM) images were attained with TECNAI G2 F20 microscope equipped with energy dispersive X-ray (EDX) at an accelerating voltage of 200 kV. The as-prepared samples were suspended in ethanol with the aid of sonication and dropped onto a carbon coated copper grid and dried at room temperature. The elemental content of the as-prepared samples, was measured using inductively coupled plasma-mass spectrometry (ICP-MS) (Agilent 7900 ICP-MS). X-ray photoelectron spectroscopy (XPS) analysis was carried out with X-ray microprobe PHI Quantera (Ulvac-PHI, INC.) equipped with monochromatic Al-Kα (hυ = 1486.6 eV) X-ray source. The optical properties of the as-synthesized photocatalyst were analyzed with diffuse reflectance absorption spectra and ultraviolet-visible spectra using Agilent Cary 100. Photoluminescence (PL) measurements were performed using LS 55 PerkinElmer fluorescence spectrophotometer with an excitation wavelength of 320 nm.

2.5. Photoelectrochemical measurements

A three electrode electrochemical quartz cell consisting a working electrode, Pt counter electrode and Ag/AgCl saturated with 3 M KCl as reference electrode was used to measure transient photocurrent responses and electrochemical impedance spectroscopy (EIS) Nyquist plots. 0.5 M Na_2SO_4 was used as an electrolyte for all the photoelectrochemical measurements. The working electrodes were prepared by suspending the samples in ethanol (1 mg/mL). The suspension solution was then drop-casted onto a fluorine-doped tin oxide (FTO) with an electroactive area of 1 cm^2. The amplitude and frequency of the AC potential were 0.01 V and 100 Hz, respectively.

2.6. Photocatalytic hydrogen production

The experiments for photocatalytic H_2 production were carried out in a black box fitted with a Pyrex reactor in a N_2 environment at room temperature and atmospheric pressure. 3 mg of the as-prepared

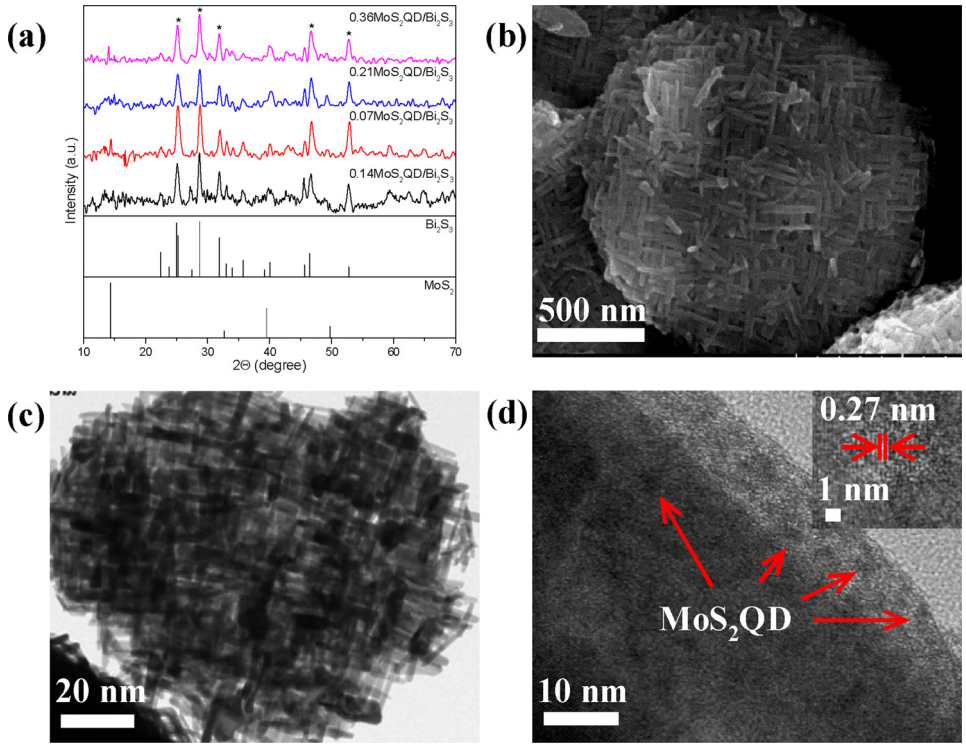

Fig. 1. (a) XRD spectra of the MoS_2QD-doped Bi_2S_3 samples synthesized with Bi_2S_3 and MoS_2 (b) FE-SEM, (c) TEM and (d) HR-TEM images of $0.14MoS_2QD/Bi_2S_3$ (Inset: lattice spacing of MoS_2QD indicating (100) plane).

photocatalyst was dispersed in 120 mL aqueous solution. 0.5 M Na_2S and 0.5 M Na_2SO_3 were used as scavenger. To ensure that the photocatalytic system was free from atmospheric air, the system was purged with N_2 gas for 30 min before the commencement of the photocatalytic reaction. The irradiation light source used in this study was a 500 W Xenon arc lamp (CHF-XM-500W) fixed with optical filter (AM1.5) to mimic solar light. The sampling port was connected to an online gas chromatography (Agilent 7890A, TCD, Ar gas carrier) to analyze the product gas at a time interval of 1 h.

3. Results and discussion

3.1. Structural and chemical characterization

The crystallographic structures of the as-developed samples were studied using XRD, as shown in Fig. 1(a). No broadening of peaks was observed for all samples, indicating their high crystallinity nature. The diffraction peaks shown in Fig. 1(a) matched well with the orthorhombic phases of Bi_2S_3 (JCPDS #012-0320), thus confirming the successful synthesis of Bi_2S_3 through the in-situ anion exchange approach. The diffraction peaks of Bi_2WO_6 were not detected across the entire prepared samples ($2\theta = 55.8^{\circ}$). This further verified the successful conversion of Bi_2WO_6 to Bi_2S_3. The reason behind the absence of MoS_2QDs diffraction peaks could be attributed to the small loading of MoS_2 on the composite materials. The structure and morphology of the as-prepared MoS_2QDs doped Bi_2S_3 were examined using FE-SEM and TEM. Fig. 1(b)–(d) shows the microscopy images of the $0.14MoS_2QD/Bi_2S_3$ sample. The FE-SEM images of 0.07, 0.21 and $0.36MoS_2QD/Bi_2S_3$ are shown in Fig. S1. These images revealed that all samples exhibited the discoid shape of Bi_2S_3, which were similar to our previous observations [29]. The average size of MoS_2QD/Bi_2S_3 samples was determined from FE-SEM to be *ca.* 1 μm. The TEM image presented in Fig. 1(c) divulged that the $0.14MoS_2QD/Bi_2S_3$ sample consisted of multiple rod-shaped structures which were stacked to form the distinct discoid shape of Bi_2S_3. The MoS_2QDs can be observed under the high resolution TEM (Fig. 1(d)) as marked by arrows. The inset of Fig. 1(d) revealed a lattice fringe of 0.27 nm, ascribed to the (100) plane of MoS_2. TEM elemental mapping of $0.14MoS_2QD/Bi_2S_3$ shown in Fig. S2 confirmed the presence of Bi, S and Mo. Furthermore, the actual MoS_2QDs content of the as-prepared samples was determined using ICP-MS and the results are presented in Table S1.

The surface valence state and surface chemical compositions of MoS_2QDs were further verified by X-ray photoelectron spectroscopy (XPS). The survey spectrum of MoS_2QD/Bi_2S_3 is shown in Fig. S3. All component elements Bi and Mo were identified in the wide scan, while no impurities were detected, indicating a high purity of the MoS_2QD/Bi_2S_3 sample. The S element peak was not visible in the survey scan of $0.14MoS_2QD/Bi_2S_3$, as it could be shielded by the Bi element. This observation is in line with other reports published in literature [30,31]. The high resolution orbit scan of individual elements is shown in Fig. 2. The peaks detected at binding energies 228.9 and 232.5 eV (Fig. 2(a)) can be ascribed to Mo $3d_{5/2}$ and Mo $3d_{3/2}$, respectively. Both Mo peaks are typical for Mo^{4+} in MoS_2 [32–34]. The peak at 225.7 eV can be assigned to S 2s. The peaks for Bi at 158.5 and 164.7 eV shown in Fig. 2(b) correspond to Bi $4f_{7/2}$ and Bi $4f_{5/2}$, respectively. Following deconvolution, the peak at binding energy of 159.5 eV can be attributed to S $2p_{3/2}$. The presence of this peak confirms the existence of S element in the MoS_2/Bi_2S_3 composite.

The optical properties of the as-synthesized samples were studied using UV–vis diffuse reflectance spectra (Fig. S4). It is evident from Fig. S4(a) that the light absorption ability of Bi_2S_3 improved significantly upon doping with MoS_2QDs instead of MoS_2 nanosheets. The light absorption ability of the samples was also observed to increase with the loading of MoS_2QDs. It is also worth mentioning that the increase in light absorption was not limited to a specific wavelength, but was observable throughout the entire scanning spectrum *i.e.* 200–800 nm. This study clearly revealed the improved photoresponsiveness of the Bi_2S_3 samples upon doping with MoS_2QDs. The band gap energy of Bi_2S_3 was also calculated by a modified Tauc plot approach (Fig. S4(b)).

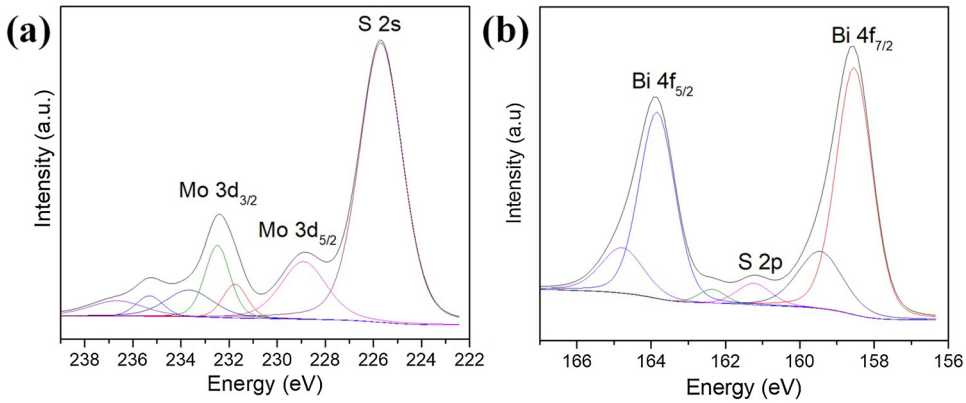

Fig. 2. XPS spectra of $0.14MoS_2QD/Bi_2S_3$ composite (a) Mo 3d and (b) Bi 4f and S 2p.

3.2. Photocatalytic H_2 production and mechanism of photocatalytic enhancement

The photocatalytic performance of the as-prepared samples were examined through the photocatalytic splitting of water under simulated solar light irradiation. The light spectrum is shown in Fig. S5. Fig. 3 shows the time-dependence H_2 yield (a) and the total product yield after 6 h of reaction (b). The results obtained revealed the importance of MoS_2QDs in improving the photocatalytic production of H_2. As shown in Fig. 3(b), pristine Bi_2S_3 produced a total H_2 yield of 3.9 mmol/g.h after 6 h of light irradiation. Upon doping with 0.07 wt% MoS_2QDs, the composite showed a H_2 production of 13.3 mmol/g.h, which was 3.4 times higher. The highest H_2 yield of 17.7 mmol/g.h was obtained when 0.14 wt% of MoS_2QD were incorporated onto Bi_2S_3. In addition to that, the quantum size of MoS_2 was also responsible for the increase in photocatalytic performance due to significantly enhanced charge separation [33]. As the exposed S atoms are active sites for H_2 production, size reduction from bulk to QDs greatly increased the S atom for H^+ adsorption to form S—H bond, giving rise to the increase in H_2 production. Further increase in the loading of QDs was found to reduce the efficiency of the photocatalyst. At higher loading of QDs, a shielding effect could have occurred, leading to the blockage of incident light from reaching the Bi_2S_3 surface. In addition to remarkable activity, high photostability is also an essential characteristic that must be possessed by a good photocatalyst. To investigate the photostability of $0.14MoS_2QD/Bi_2S_3$, its performance in the photocatalytic production of H_2 was evaluated for four consecutive runs under identical experimental conditions. As shown in Fig. 3(c) and (d), the photoactivity of $0.14MoS_2QD/Bi_2S_3$ was maintained after four cycles with a total reaction time of 24 h. $0.14MoS_2QD/Bi_2S_3$ was able to retain more than 90%

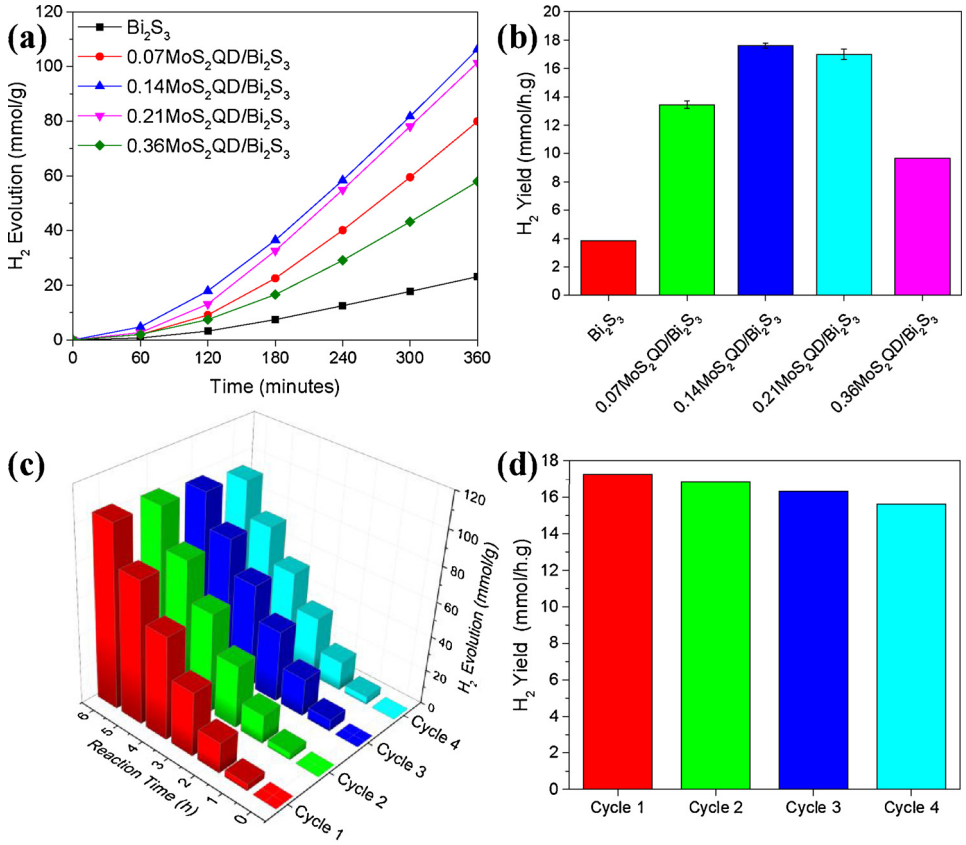

Fig. 3. (a) Time course of photocatalytic H_2 evolution, (b) rate of photocatalytic H_2 production of all samples, (c) time course for 4 cycles of photocatalytic H_2 production over $0.14MoS_2QD/Bi_2S_3$ and (d) rate of H_2 production for each cycles studied in 0.5 M Na_2S/Na_2SO_3 mixture under stimulated solar light irradiation for duration of 6 h.

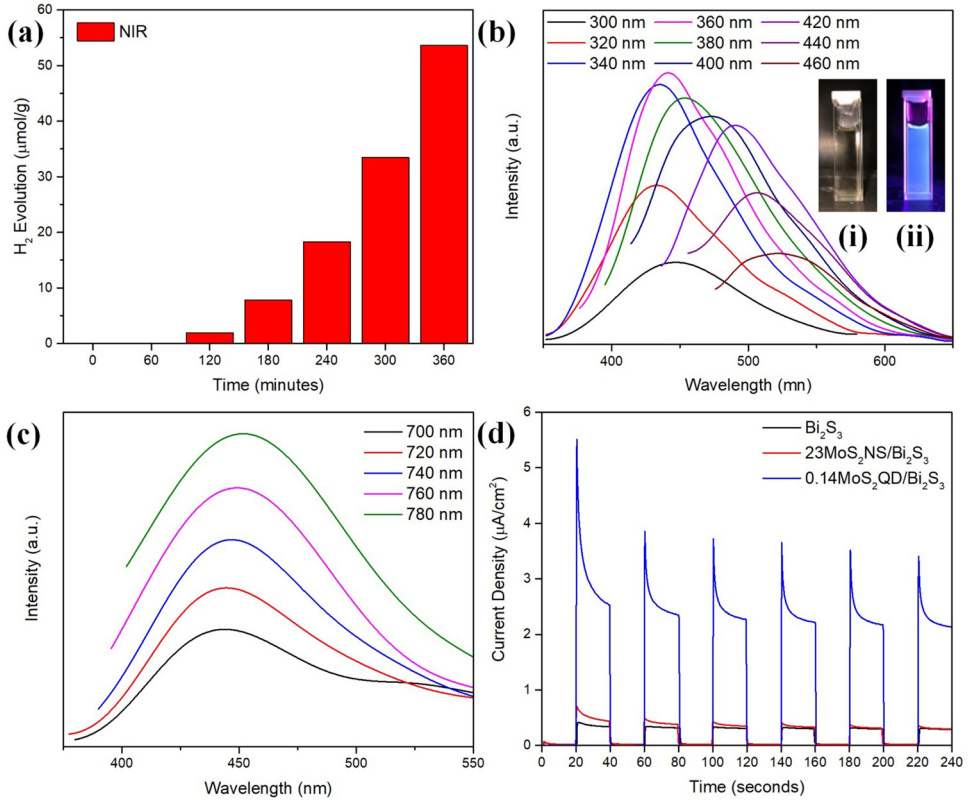

Fig. 4. (a) H_2 evolution of $0.14MoS_2QD/Bi_2S_3$ under NIR irradiation, (b) down-converted (Inset: MoS_2QDs under (i) visible and (ii) UV light irradiation), (c) up-converted PL spectra of MoS_2QDs, and (d) transient photocurrent response under NIR irradiation.

of photoactivity after 4 consecutive reaction run, thus indicating its superior photostability.

To verify the activity of MoS_2QD/Bi_2S_3 photocatalyst under NIR light ($\lambda > 700$ nm), $0.14MoS_2QD/Bi_2S_3$ was subjected to photocatalytic H_2 production under similar reaction conditions, but under NIR light illumination instead. The results, as presented in Fig. 4(a), showed that MoS_2QDs were able to harness the NIR light for H_2 production through water splitting. In order to understand the significance of this result, PL characterization was carried out on MoS_2QDs. Fig. 4(b) and (c) show the PL emission spectra of the MoS_2QDs under different excitation wavelength, which disclosed the as-synthesized MoS_2QDs exhibited intriguing excitation-dependent PL emission properties. This suggests that MoS_2QDs not only acted as spectral harvesters, they also played a pivotal role as excellent spectral converters. This phenomenon could be attributed to the homogeneity of the as-developed MoS_2QDs, further confirming the successful synthesis of quantum-sized MoS_2 through the facile sonochemical approach. In addition to the down-converted PL property, MoS_2QDs also possess fascinating up-converted PL behavior as shown in Fig. 4(c). Upon excitation under NIR irradiation (700–780 nm), the PL emission spectra were found to be in the range of 440–455 nm. This suggested that the as-fabricated MoS_2QDs could up-convert long-wavelength NIR light to short-wavelength visible light. This is exceptionally desirable in photocatalysis as it manifests that NIR region could also be harvested, hence maximizing the utilization of the solar spectrum. Although MoS_2QDs suspension appeared as light brown solution under visible light irradiation, the MoS_2QDs emitted bright blue light under UV irradiation, as displayed in Fig. 4(b) insets. This observation revealed that the MoS_2QDs possessed strong fluorescence emissions [35,36]. The photoactivity of $0.14MoS_2QD/Bi_2S_3$ was further verified with transient photocurrent responses carried out under NIR irradiation. The results obtained were presented in Fig. 4(d). The photocatalyst decorated with MoS_2QDs showed strong photocurrent response under NIR irradiation. As a comparison, similar characterization was carried out for pristine Bi_2S_3 and MoS_2 nanosheets grown directly onto Bi_2S_3 ($23MoS_2NS/Bi_2S_3$). As shown in Fig. 4(d), the photocurrent response of pristine Bi_2S_3 and $23MoS_2NS/Bi_2S_3$ were significantly lower than that for $0.14MoS_2QD/Bi_2S_3$. This observation clearly indicates the superiority of MoS_2QDs under NIR irradiation. Refer to ESI and Fig. S6 for the justifications of selection of $23MoS_2NS/Bi_2S_3$ as a control sample. Further experiments were carried out to investigate the effects of MoS_2 structure on the photocatalytic activity. As presented in Fig. S7, when bulk MoS_2 was used as photocatalyst for H_2 water splitting, a negligible amount of H_2 was produced. For $23MoS_2NS/Bi_2S_3$, 6.1 mmol/g.h of H_2 was yielded under similar experimental conditions. The enhancement in photoactivity was due to the intimate contact between MoS_2 and Bi_2S_3, which allowed rapid transfer and migration of photoinduced electrons and the subsequent suppression of electron-hole pair recombination [28]. When MoS_2QDs were incorporated in place of MoS_2 nanosheets, the H_2 production increased to a whopping 17.7 mmol/g.h. The yield obtained was 4.5- and 2.9-folds higher than that of undoped Bi_2S_3 and $23MoS_2NS/Bi_2S_3$, respectively. This showed that only 0.14 wt% of MoS_2QDs was required to produce H_2 yield with almost 3-fold higher than that of 23 wt% of MoS_2NS used.

Electrochemical impedance spectroscopy (EIS) Nyquist plots of the samples are presented in Fig. 5(a). The charge transfer resistance between the contact interface, working electrode and electrolyte was revealed by the arc radius from the Nyquist plot. The arc radius of $0.14MoS_2QD/Bi_2S_3$ reduced significantly as compared to undoped Bi_2S_3 and $23MoS_2NS/Bi_2S_3$ (see Fig. S8(a)). This implicates the importance of MoS_2QDs on the photoactivity of Bi_2S_3. As the loading of MoS_2QDs increased from 0.07 wt% to 0.14 wt%, the charge transfer resistance between the surface of the electrode and the electrolyte reduced. This observation implied a more efficient interfacial charge transfer within the composite. However, a further increase in MoS_2QDs loading caused an increase in electron charge transfer resistance. Therefore, a balance

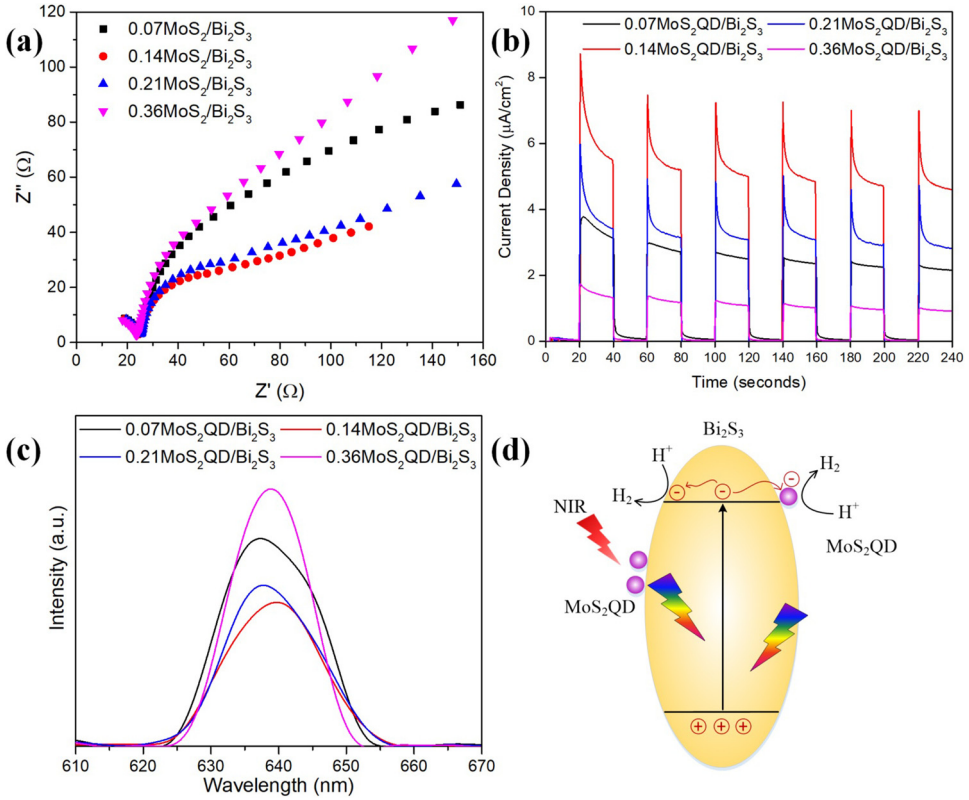

Fig. 5. (a) EIS Nyquist plots, (b) transient photocurrent response under simulated solar light, (c) steady-state PL spectra of the as-prepared MoS_2QDs doped samples and (d) schematic illustration of H_2 production under light irradiation.

between charge transfer mobility and electron hole recombination is desirable, and this was attained when 0.14wt% of MoS_2QDs was doped onto Bi_2S_3.

To further verify the results, transient photocurrent responses were performed on the as-prepared samples (see Fig. 5(b)). The current density was observed to have increased as soon as the light was switched on; photocurrent responses decreased to near zero when the light was turned off. In accordance to the photocatalytic experiments, 0.14MoS_2QD/Bi_2S_3 showed the highest photocurrent responses to the on/off light irradiation cycles as compared to the other loadings of MoS_2QDs. This indicated that more electrons were able to migrate to the electrodes to produce a current flow. In addition, 0.14MoS_2QD/Bi_2S_3 showed superiority in transient photocurrent responses in comparison to undoped Bi_2S_3 and 23MoS_2NS/Bi_2S_3 (Fig.S8(b)), demonstrating efficient separation of photogenerated charges. Photoluminescence (PL) analysis is shown in Fig. 5(c). Suppression of the emission peak for 0.14MoS_2QD/Bi_2S_3 signified the delay in electron-hole pair recombination of the photocatalyst. As compared to 0.07, 0.21 and 0.36 wt% of MoS_2QDs loading, the electron-hole recombination rate of 0.14MoS_2QD/Bi_2S_3 was the lowest, indicating that 0.14MoS_2QD/Bi_2S_3 was the most efficient composite for charge separation. This observation matches well with the H_2 production results reported earlier. Fig. S8(c) shows the PL spectra for the as-synthesized MoS_2 doped samples in this study. The spectra showed that 0.14MoS_2QD/Bi_2S_3 had the lowest peak intensity as compared to the other samples. This further demonstrated the significance of the MoS_2 structure, in which quantum dots were more efficient in suppressing electron-hole recombination, which in turn resulted in higher H_2 yield.

The schematic illustration of the photoexcited electron-hole pair separation for 0.14MoS_2QD/Bi_2S_3 is presented in Fig. 5(d). Under light irradiation, electrons on Bi_2S_3 were excited from the VB to the CB, which then reacted with adsorbed H^+ ions to form H_2 molecules. The enhancement of the photocatalytic production of H_2 can be attributed to the synergetic effect between MoS_2QDs and Bi_2S_3 where the photogenerated electrons on Bi_2S_3 could transfer to MoS_2QDs to take part in the H_2 production reaction. Furthermore, as a spectral converter, the MoS_2QDs were capable of harnessing NIR light to drive the photocatalytic H_2 production. Through this, Bi_2S_3 could utilize the up-converted light to excite electrons from the ground state for water reduction. Besides, the addition of MoS_2QDs enhanced the visible light absorption and promoted charge transfer and separation, giving the photocatalyst a longer reaction lifetime.

4. Conclusion

In summary, MoS_2QDs decorated Bi_2S_3 was successfully synthesized *via* a facile hydrothermal method. The presence of MoS_2QDs has effectively enhanced the photocatalytic H_2 evolution for all samples. At an optimum loading of 0.14 wt% of MoS_2QDs, the H_2 evolution rate was the highest at 17.7 mmol/g.h. The improvement was found to be 3.0- and 4.5-fold higher than that of control 23MoS_2NS/Bi_2S_3 and undoped Bi_2S_3, respectively. The enhancement is due to the synergistic effects between Bi_2S_3 and MoS_2QDs, in which the MoS_2QDs played bifunctional roles as electron entrapment sites and spectral converters. This work demonstrated the importance of MoS_2QDs and their potential in replacing noble metal co-catalysts for photocatalytic H_2 production under broad solar spectrum. MoS_2QD/Bi_2S_3 photocatalyst paves a new pathway for utilizing solar spectrum for H_2 production and a step closer to the realization of a fossil fuel-free world.

Acknowledgements

This work was financially supported by Monash University Malaysia under Advanced Engineering Platform; and the Ministry of Higher Education (MOHE) Malaysia and Universiti Sains Malaysia (USM) under NanoMITe Long-term Research Grant Scheme (LRGS) (Ref no.:

203/PJKIMIA/6720009).

Appendix A. Supplementary data

Supplementary material related to this article can be found, in the online version, at doi:10.1016/j.apcatb.2018.03.019.

References

[1] X. Jin, X. Fan, J. Tian, R. Cheng, M. Li, L. Zhang, MoS_2 quantum dot decorated g-C_3N_4 composite photocatalyst with enhanced hydrogen evolution performance, RSC Adv. 6 (2016) 52611–52619.

[2] C. Ma, H. Zhu, J. Zhou, Z. Cui, T. Liu, Y. Wang, Y. Wang, Z. Zou, Confinement effect of monolayer MoS_2 quantum dots on conjugated polyimide and promotion of solar-driven photocatalytic hydrogen generation, Dalton Trans. 46 (2017) 3877–3886.

[3] F.A. Frame, F.E. Osterloh, CdSe-MoS_2: a quantum size-confined photocatalyst for hydrogen evolution from water under visible light, J. Phys. Chem. C 114 (2010) 10628–10633.

[4] B.-J. Ng, L.K. Putri, L.-L. Tan, P. Pasbakhsh, S.-P. Chai, All-solid-state Z-scheme photocatalyst with carbon nanotubes as an electron mediator for hydrogen evolution under simulated solar light, Chem. Eng. J. 316 (2017) 41–49.

[5] L.K. Putri, B.-J. Ng, W.-J. Ong, H.W. Lee, W.S. Chang, S.-P. Chai, Heteroatom nitrogen- and boron-doping as a facile strategy to improve photocatalytic activity of standalone reduced graphene oxide in hydrogen evolution, ACS Appl. Mater. Interfaces 9 (2017) 4558–4569.

[6] L.-L. Tan, W.-J. Ong, S.-P. Chai, A.R. Mohamed, Visible-light-activated oxygen-rich TiO_2 as next generation photocatalyst: importance of annealing temperature on the photoactivity toward reduction of carbon dioxide, Chem. Eng. J. 283 (2016) 1254–1263.

[7] M.-Y. Xie, K.-Y. Su, X.-Y. Peng, R.-J. Wu, M. Chavali, W.-C. Chang, Hydrogen production by photocatalytic water-splitting on Pt-doped TiO_2–ZnO under visible light, J. Taiwan Inst.Chem. Eng. 70 (2017) 161–167.

[8] Z. Zhu, C.-T. Kao, B.-H. Tang, W.-C. Chang, R.-J. Wu, Efficient hydrogen production by photocatalytic water-splitting using Pt-doped TiO_2 hollow spheres under visible light, Ceram. Int. 42 (2016) 6749–6754.

[9] E.A. Kozlova, A.Y. Kurenkova, P.A. Kolinko, A.A. Saraev, E.Y. Gerasimov, D.V. Kozlov, Photocatalytic hydrogen production using Me/$Cd_{0.3}Zn_{0.7}S$ (Me = Au, Pt, Pd) catalysts: transformation of the metallic catalyst under the action of the reaction medium, Kinet. Catal. 58 (2017) 431–440.

[10] S.Y. Arzate Salgado, R.M. Ramírez Zamora, R. Zanella, J. Peral, S. Malato, M.I. Maldonado, Photocatalytic hydrogen production in a solar pilot plant using a Au/TiO_2 photo catalyst, Int. J. Hydrogen Energy 41 (2016) 11933–11940.

[11] J. Qin, J. Huo, P. Zhang, J. Zeng, T. Wang, H. Zeng, Improving the photocatalytic hydrogen production of Ag/g-C_3N_4 nanocomposites by dye-sensitization under visible light irradiation, Nanoscale 8 (2016) 2249–2259.

[12] Y. Tang, W. Di, X. Zhai, R. Yang, W. Qin, NIR-responsive photocatalytic activity and mechanism of $NaYF_4$:Yb,Tm@TiO_2 core–shell nanoparticles, ACS Catal. 3 (2013) 405–412.

[13] M. Tou, Y. Mei, S. Bai, Z. Luo, Y. Zhang, Z. Li, Depositing CdS nanoclusters on carbon-modified $NaYF_4$:Yb,Tm upconversion nanocrystals for NIR-light enhanced photocatalysis, Nanoscale 8 (2016) 553–562.

[14] M. Zhu, X. Cai, M. Fujitsuka, J. Zhang, T. Majima, Au/$La_2Ti_2O_7$ nanostructures sensitized with black phosphorus for plasmon-enhanced photocatalytic hydrogen production in visible and near-infrared light, Angew. Chem. Int. Ed. 56 (2017) 2064–2068.

[15] Z. Zheng, T. Tachikawa, T. Majima, Single-particle study of Pt-modified Au nanorods for plasmon-enhanced hydrogen generation in visible to near-infrared region, J. Am. Chem. Soc. 136 (2014) 6870–6873.

[16] W. Xing, Y. Chen, X. Wang, L. Lv, X. Ouyang, Z. Ge, H. Huang, MoS_2 quantum dots with a tunable work function for high-performance organic solar cells, ACS Appl. Mater. Interfaces 8 (2016) 26916–26923.

[17] J. Kibsgaard, Z. Chen, B.N. Reinecke, T.F. Jaramillo, Engineering the surface structure of MoS_2 to preferentially expose active edge sites for electrocatalysis, Nat. Mater 11 (2012) 963–969.

[18] S. Wang, X. Li, Y. Chen, X. Cai, H. Yao, W. Gao, Y. Zheng, X. An, J. Shi, H. Chen, A facile one-pot synthesis of a two-dimensional MoS_2/Bi_2S_3 composite theranostic nanosystem for multi-modality tumor imaging and therapy, Adv. Mater. 27 (2015) 2775–2782.

[19] Y. Li, L. Wang, T. Cai, S. Zhang, Y. Liu, Y. Song, X. Dong, L. Hu, Glucose-assisted synthesize 1D/2D nearly vertical CdS/MoS_2 heterostructures for efficient photocatalytic hydrogen evolution, Chem. Eng. J. 321 (2017) 366–374.

[20] T.P. Nguyen, W. Sohn, J.H. Oh, H.W. Jang, S.Y. Kim, Size-dependent properties of two-dimensional MoS_2 and WS_2, J. Phys. Chem. C 120 (2016) 10078–10085.

[21] R. Ganatra, Q. Zhang, Few-layer MoS_2: a promising layered semiconductor, ACS Nano 8 (2014) 4074–4099.

[22] X. Meng, Z. Li, H. Zeng, J. Chen, Z. Zhang, MoS_2 quantum dots-interspersed Bi_2WO_6 heterostructures for visible light-induced detoxification and disinfection, Appl. Catal. B. 210 (2017) 160–172.

[23] D. Wang, Y. Xu, F. Sun, Q. Zhang, P. Wang, X. Wang, Enhanced photocatalytic activity of TiO_2 under sunlight by MoS_2 nanodots modification, Appl. Surf. Sci. 377 (2016) 221–227.

[24] X. Hao, Z. Jin, H. Yang, G. Lu, Y. Bi, Peculiar synergetic effect of MoS_2 quantum dots and graphene on metal-organic frameworks for photocatalytic hydrogen evolution, Appl. Catal. B. 210 (2017) 45–56.

[25] X. Wang, S. Chen, M. Zhang, Y. Huang, S. Feng, D. Zhao, MoS_2 quantum dot-modified Ag/polyaniline composites with enhanced photogenerated carrier separation for highly efficient visible light photocatalytic H_2 evolution performance, Catal. Sci. Tech. (2017).

[26] H. Huang, C. Du, H. Shi, X. Feng, J. Li, Y. Tan, W. Song, Water-soluble monolayer molybdenum disulfide quantum dots with upconversion fluorescence, Part. Part. Syst. Charact. 32 (2015) 72–79.

[27] W. Gu, Y. Yan, C. Zhang, C. Ding, Y. Xian, One-step synthesis of water-soluble MoS_2 quantum dots via a hydrothermal method as a fluorescent probe for hyaluronidase detection, ACS Appl. Mater. Interfaces 8 (2016) 11272–11279.

[28] W.P.C. Lee, M.-M. Gui, L.-L. Tan, T.Y. Wu, S. Sumathi, S.-P. Chai, Bismuth sulphide-modified molybdenum disulphide as an efficient photocatalyst for hydrogen production under simulated solar light, Catal. Commun. 98 (2017) 66–70.

[29] W.P.C. Lee, F.-H. Wong, N.K. Attenborough, X.Y. Kong, L.-L. Tan, S. Sumathi, S.-P. Chai, Two-dimensional bismuth oxybromide coupled with molybdenum disulphide for enhanced dye degradation using low power energy-saving light bulb, J. Environ. Manag. 197 (2017) 63–69.

[30] N. Liang, J. Zai, M. Xu, Q. Zhu, X. Wei, X. Qian, Novel Bi_2S_3/$Bi_2O_2CO_3$ heterojunction photocatalysts with enhanced visible light responsive activity and wastewater treatment, J. Mater. Chem. A 2 (2014) 4208–4216.

[31] A. Rauf, M.S.A. Sher Shah, G.H. Choi, U.B. Humayoun, D.H. Yoon, J.W. Bae, J. Park, W.-J. Kim, P.J. Yoo, Facile synthesis of hierarchically structured Bi_2S_3/Bi_2WO_6 photocatalysts for highly efficient reduction of Cr(VI), ACS Sustain. Chem. Eng. 3 (2015) 2847–2855.

[32] B.A. Vanchura, P. He, V. Antochshuk, M. Jaroniec, A. Ferryman, D. Barbash, J.E. Fulghum, S.D. Huang, Direct synthesis of mesostructured lamellar molybdenum disulfides using a molten neutral n-alkylamine as the solvent and template, J. Am. Chem. Soc. 124 (2002) 12090–12091.

[33] W. Gao, M. Wang, C. Ran, L. Li, Facile one-pot synthesis of MoS_2 quantum dots-graphene-TiO_2 composites for highly enhanced photocatalytic properties, Chem. Commun. 51 (2015) 1709–1712.

[34] F. Liu, Y. Jiang, J. Yang, M. Hao, Z. Tong, L. Jiang, Z. Wu, MoS_2 nanodot decorated In_2S_3 nanoplates: a novel heterojunction with enhanced photoelectrochemical performance, Chem. Commun. 52 (2016) 1867–1870.

[35] S. Kumar, A.K. Ojha, B. Ahmed, A. Kumar, J. Das, A. Materny, Tunable (violet to green) emission by high-yield graphene quantum dots and exploiting its unique properties towards sun-light-driven photocatalysis and supercapacitor electrode materials, Mater. Today Commun. 11 (2017) 76–86.

[36] X.Y. Kong, W.L. Tan, B.-J. Ng, S.-P. Chai, A.R. Mohamed, Harnessing vis–NIR broad spectrum for photocatalytic CO_2 reduction over carbon quantum dots-decorated ultrathin Bi_2WO_6 nanosheets, Nano Res. 10 (2017) 1720–1731.